ABSTRACT

Title of Document: SYNTHESIS AND CHARACTERIZATIONS OF OXIDIZERS FOR BIOCIDAL NANOENERGETIC APPLICATIONS

Jingyu Feng, Master of Science, 2013

Directed By: Professor Michael R. Zachariah, Department of Chemical Engineering and Chemistry

Nanoenergetic materials have been shown to have reactive properties superior to traditional energetic materials since the nanoscale enables more intimate mixing of fuel and oxidizer to reduce the heat and mass transport limitations. The growing threat of biological weapons has prompted research efforts into new energetic materials with biocidal capabilities. Most notably the biocidal nanothermite involves the aluminum fuel with a strong oxidizer, which releases the biocide. In this thesis two kinds of attempted synthesis and characterizations were covered for this biocidal nanoenergetic topic: (1) the highly hygroscopic strong oxidizer I_2O_5 was successfully passivated into the Fe_2O_3 shell, which exhibited excellent combustion performance with biocidal capabilities when formulated into aluminum based nanothermite reaction; (2) the copper iodate and iron iodate particles were prepared by co-precipitation and demonstrated to be good candidates for the potential biocidal energetic applications.

SYNTHESIS AND CHARACTERIZATIONS OF OXIDIZERS FOR BIOCIDAL NANOENERGETIC APPLICATIONS

By

Jingyu Feng

Thesis submitted to the Faculty of the Graduate School of the
University of Maryland, College Park, in partial fulfillment
of the requirements for the degree of
Master of Science
2013

Advisory Committee:
Professor Michael R. Zachariah, Chair
Professor Philip DeShong
Professor Bryan Eichhorn
Professor Zhihong Nie

Dedication

This work is dedicated to my parents and my wife

Acknowledgements

I would like to express my deepest gratitude to my advisor Dr. Michael R. Zachariah. During my master study, Dr. Michael R. Zachariah led me to this new research area and kept guiding, encouraging and supporting me to conduct research; working with him has been a great experience and memory of my entire life. Without his guidance, I wouldn't have finished this thesis work.

I would like to thank Professor Philip DeShong, Professor Bryan Eichhorn, and Professor Zhihong Nie for their time to serve on my thesis committee. I would also thank Dr. Li-Chung Lai and Dr. Wen-An Chiou in Maryland NanoCenter for helping to do TEM and EDS line scan.

I would like to thank all my friends and colleagues in University of Maryland College Park, especially I would like to thank Guoqiang Jian, Fangyu Cao, Dr. Qing Liu, Dr. Lei Zhou, Dr. Mingdong Li, and Dr. Xiaofei Ma, who I worked with and helped me a lot with experiments in laboratory. In addition, I appreciate other group members in Dr. Michael R. Zachariah's group; I really enjoy working and discussing with them.

Table of Contents

List of Tables

List of Figures

Chapter 1: Introduction and Background

1.1 Nanothermite

Energetic materials, basically a class of materials that store significant quantities of energy [1], are widely used in various military and civilian applications such as explosives, pyrotechnics, and propellants etc. Fundamentally energetic materials are the mixture of both fuel and oxidizer, which can be categorized into the following two groups: (1) the conventional explosives are usually single organic molecules, such as nitrocellulose, trinitrotoluene (TNT) and cyclotrimethylenetrinitramine (RDX); (2) the thermite, highly exothermic, is a mixture of metal fuel and oxidizer:

$$M + AO \rightarrow MO + A + \Delta H \text{ …….. (a)}$$

In the equation (a), M is the metal fuel while AO is the oxidizer and ΔH is the energy release of the thermite reaction. Aluminum is commonly used as metal fuel in thermite reaction because it is cheap and its enthalpy of combustion is very high [2,3]. The "traditional" thermite is the stoichiometric mixture of aluminum powder and Fe_3O_4 powder reacting completely to produce iron and alumina (Al_2O_3).

The energy density is defined as the energy release ΔH per unit volume ΔH_{Volume} or unit mass ΔH_{Mass} in Figure 1. For the conventional explosives, the fuel and oxidizer are incorporated into one molecule, leading to faster reaction; however, the thermites have much higher energy density than monomolecular energetic materials, as shown in Figure 1.

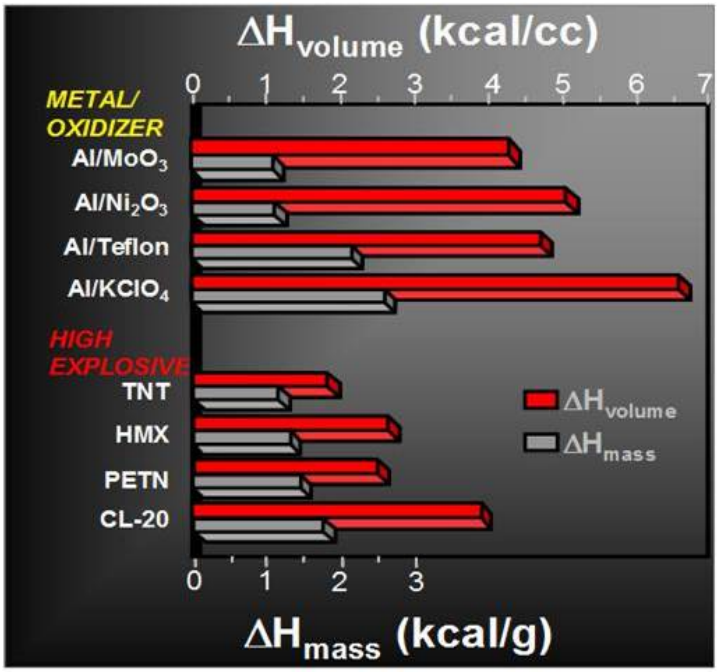

Figure 1. Energy density of thermite mixtures along with some conventional explosives [4]

When the particle sizes are reduced to the nanosized dimension (Figure 2), the intimate mixing of the metal fuel and oxidizer could be achieved, which enables a huge amount of energy output with a faster energy releasing rate as well as a higher burning rate, due to larger contact area between reactants and smaller diffusion length of both heat and mass transfer [1, 5-10].

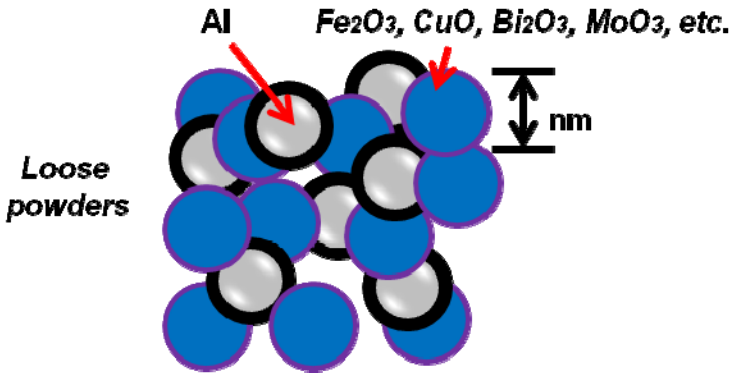

Figure 2. A scheme drawing of a nanothermite

1.2 Biocidal Application and Iodine-containing Materials

The threat of biological weapons, which attracts more and more attentions nowadays, has become one of the top five threats to the national security [11]. The possibility of a terrorist attack dispersing aerosolized biological agents would be especially difficult to predict, detect, or prevent [12]. On December 7 of 2011, at the European headquarters of the United Nations (UN) in Geneva, Switzerland, the United States warned that the terror threat from biological weapons is growing and called for closer international cooperation to prevent the threat [13].

The research efforts have been prompted into development of the new energetic materials with biocidal capabilities to inactivate the harmful microorganisms, which could be potentially used to neutralize biological weapons [14-20]. It is desired that such materials could release thermal energy like highly exothermic thermite, but also deliver long lasting biocidal event e.g., silver and halogen, because some biological agents may survive an explosion or fire [21]. Fundamentally the energetic materials consist of both fuel and oxidizer. Then the silver or halogen can be either formulated into the fuel or the oxidizer. One way, for example, is to develop nanocomposite aluminum-halogen materials to replace pure aluminum as the metal fuel in nanoenergetic formulations. Zhang *et al.* prepared a composite AlI_x by mechanical milling of aluminum and iodine to stabilize the iodine by aluminum matrix [14,15]. The elemental iodine can be released when the materials are heated and ignited. Another approach is to find a strong oxidizer, which could release biocide in aluminum based thermite reaction. Clark *et al.* investigated three oxidizers for the spore neutralization, I_2O_5, Ag_2O and Fe_2O_3 [18], and found out the iodine-containing

thermite Al+I_2O_5 was extremely effective to neutralize spores. Other possible oxidizers like $AgIO_3$, Ag_2O were also studied experimentally [19,20]. $AgIO_3$ thermally decomposes to release iodine and oxygen. Ag_2O can yield high amount of silver in Al based thermite reactions when combined with CuO and $AgIO_3$.

The iodine-containing oxidizers work ideally for this biocidal application when formulated into thermite, mainly because the iodine is an established spore-killing agent at elevated temperatures and near room temperature [22]. The released elemental iodine works as a biocide since it penetrates cell walls of micro-organisms such as bacteria, viruses, fungi and oxidizes a number of critical components within the cell to cause the death of cell. Besides, the iodine is easy to vaporize and the iodine component in the oxidizer can be completely released after thermite reaction.

1.3 Aerosol Processing

Aerosol spray pyrolysis is a low-cost and simple method which involves a limited number of preparation steps allowing for on-line continuous production of the powder and thin film [23]. Thus it has been extensively applied in various fields like food industries, pharmaceutical productions and materials processing [24].

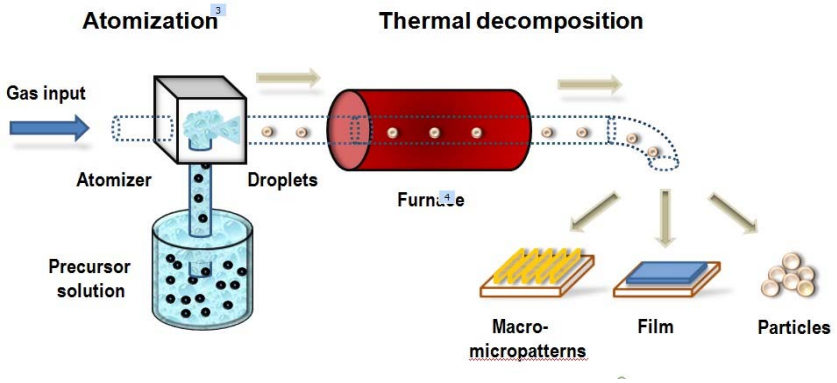

Figure 3. Aerosol spray pyrolysis process

Aerosol spray-pyrolysis includes two fundamental steps: (1) the atomization generating aerosols and (2) the pyrolysis thermally decomposing the precursor (Figure 3). In the atomization step, the atomizer disintegrates the precursor solution into droplets. Different atomizers, for example, jet atomizer, swirl atomizer and pneumatic atomizer, generate droplets following various principles [25]. After the formation, droplets are dispersed in the carrier gas, which is named as "aerosol". A series of changes will take place when aerosol goes through the furnace (Figure 4): the solvent evaporation, solutes diffusion, precipitation, decomposition and densification.

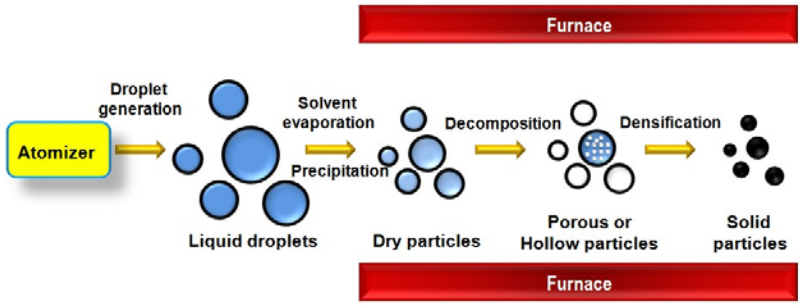

Figure 4. Thermal decomposition process in the aerosol spray pyrolysis

Additionally, when combined with controlled deposition techniques, the aerosol spray pyrolysis can directly write metal oxides on various substrates like silicon wafers, or glass slides to get the macro- or micro-patterns [26]. In the aerosol processing, each droplet is a micro-reactor and all the chemical reactions occur inside, which enables an easy control of the composition of final product.

Since our aerosol synthesis experiment is based on droplet-to-particle principle, the average size of the final particles can be roughly determined by the aerosol droplet size and the initial concentration of the starting solution [27]. For our home-

made collison type atomizer, the geometric mean diameter of the droplet, measured by a laser aerosol spectrometer, is around 1 micron [28]. Assuming that during the thermal decomposition process, the solutes are non-volatile and the final particle is spherical, the following equations could be used for the calculation of the final particle diameter:

$$\text{Volume of a single droplet:} \quad V = \frac{1}{6}\pi(1\mu m)^3$$

$$\text{Diameter of the final particle:} \quad d_p = \sqrt[3]{\frac{6C \cdot V \cdot Mw}{\rho\pi}}$$

In the above equations, C is the concentration of precursor solution. ρ is the final product density. Mw is the molecular weight of non-volatile solute in precursor solution. The morphology of particles generated by aerosol spray pyrolysis is affected by several parameters such as the properties of precursor solution, carrier gas flow rate (the residence time of heating), the solvent evaporation rate, and the furnace temperature [29]. For example, in the solvent evaporation and solute diffusion step of aerosol spray pyrolysis process as shown in Figure 5, when the solvent evaporation characteristic time τ_{sv} is much smaller than the solute diffusion characteristic time τ_{sl}, a shell could be formed on the surface of the droplet. Conversely, the solid particle formation will be obtained. The particle morphology, such as solid and spherical particles, hollow or fragmented particles (Figure 5), can be determined by transmission electron microscopy (TEM) images.

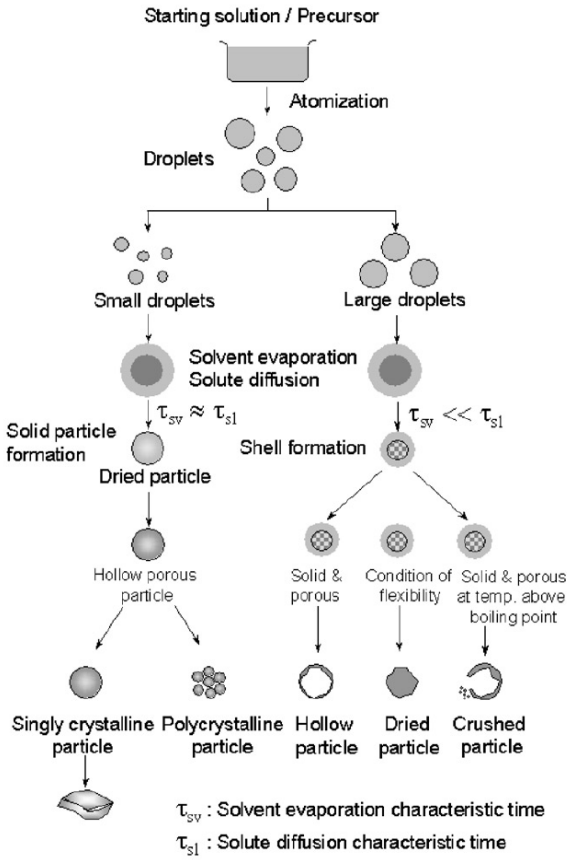

Figure 5. Particle morphology prepared by aerosol spray pyrolysis [30]

1.4 The Scope of this Thesis

As discussed previously in the introduction, the iodine-containing oxidizers work ideally for spore neutralization. The objective of this thesis is to prepare iodine-containing oxidizers for nanothermite reaction, which has potential applications in the destruction of biological agents like spores [31]. Two kinds of attempted synthesis and characterizations were covered for this biocidal nanoenergetic topic: (1) modified aerosol routes to air-stable passivated I_2O_5; (2) co-precipitation to produce copper iodate and iron iodate particles.

Iodine pentoxide (I_2O_5), also known as diiodine pentoxide, is a strong iodine-containing oxidizer for nanoenergetic applications [18], whose combustion releases

elemental iodine as a biocidal agent. However, its high hygroscopicity [32,33] hinders its combustion performance and iodine release. Chapter 2 describes a novel gas phase assisted aerosol spray-pyrolysis method to solve this problem [34]. Using this method we successfully passivated I_2O_5 into the iron oxide shell which protects I_2O_5 from the water in the ambient air. Unlike the polymer coating that can jeopardize I_2O_5's combustion performance in thermite reaction; the iron oxide shell is an active oxidizer layer reacting with aluminum in the thermite reaction. The core/shell structure was confirmed by TEM coupled with an energy dispersive X-ray spectrometer (EDS) line scan. We found that the reactivity of the final materials can be tuned by varying the Fe/I molar ratio, which is corresponded to the coating thickness.

The work in Chapter 3 was motivated by the decomposition mechanism of metal iodate [35,36] in equation (b) and (c):

$$2Cu(IO_3)_2 \rightarrow 2CuO + 2I_2 \uparrow + 5O_2 \uparrow \ldots\ldots \text{(b)}$$

$$4Fe(IO_3)_3 \rightarrow 2Fe_2O_3 + 6I_2 \uparrow + 15O_2 \uparrow \ldots\ldots \text{(c)}$$

Compared to the metal oxide counterparts, the metal iodates, such as $Fe(IO_3)_3$ and $Cu(IO_3)_2$, embrace the promise of better combustion performance with biocidal properties due to the fact that they have extra oxygen and iodine release when decomposed, which could work as the metal oxide combined with oxygen and iodine for the nanothermite formulation. In Chapter 3 $Fe(IO_3)_3$ and $Cu(IO_3)_2$ particles were synthesized and confirmed by X-ray diffraction (XRD). Their size and morphology was characterized by scanning electron microscopy (SEM). Temperature-Jump mass spectroscopy (T-Jump MS) shows a significant release of iodine and oxygen when

copper iodate was decomposed. The nanothermite formulations based on these two metal iodates particles were evaluated in the combustion cell test and compared with reference CuO and Fe_2O_3 particles.

Chapter 2: Passivated I_2O_5 for Potential Biocidal Nanoenergetic Applications

1. Introduction

The motivation of this work is based on the fact that I_2O_5 is a strong, iodine-containing oxidizer for biocidal energetic application but it is highly hygroscopic. After exposing to the air, I_2O_5 can react with water to form iodic acid HIO_3. As a strong acid, HIO_3 could react with aluminum when mixing and thus deactivate the thermite reaction. To solve this problem, the coating on the I_2O_5 surface was needed.

A single step, two-furnace aerosol strategy was developed by Prakash *et al.* in our group to create a core/shell structured nanocomposite oxidizer for thermite reaction [37]. In such material a strong oxidizer ($KMnO_4$) was coated with a thin layer of weak oxidizer Fe_2O_3. In this strategy, the iron nitrate and potassium permanganate solution was sprayed into aerosol droplets which passed through sequentially the silica-gel diffusion dryer and two tube furnaces at 120 °C and 240 °C. $Fe(NO_3)_3$ decomposed to Fe_2O_3 while permanganate remained solid at 120 °C. Then at 240 °C $KMnO_4$ then melted and Fe_2O_3 began to aggregate as a shell surrounding the permanganate core. The reactivity of the final materials was determined by the thickness of Fe_2O_3 coating layer [37]. To further extend the application of this strategy, Wu *et al.* in our group utilized this process to successfully encapsulate strong oxidizer $KClO_4$ and NH_4ClO_4 with Fe_2O_3 and CuO shell [38]. Here the key to the process is based on that in the aerosol processing aerosol droplet works as a

micro-reactor where all the physical and chemical processes take place and the characteristic temperatures of the two precursors are different.

The above-mentioned two-furnace strategy is appealing to create passivated I_2O_5 particles. Unfortunately, the shell precursors $Fe(NO_3)_3$ and $Cu(NO_3)_2$ react immediately with HIO_3, I_2O_5's precursor, to form precipitates in water. In this Chapter, we developed a modified gas phase assisted aerosol synthesis approach to successfully passivate I_2O5 within the iron oxide shell to create an air-stable I_2O_5/Fe_2O_3 nanocomposite oxidizer, which was confirmed by the mass spectra (MS) obtained during the rapid heating and TEM associated with EDS line scan. These materials were then formulated into nanoaluminum based thermite mixtures to evaluate their combustion performance. The passivated oxidizers exhibited good stability when exposed to ambient air in the long term stability experiment.

2.Experimental Details

2.1. Materials

Iodic acid (HIO_3, 99.5%), iron pentacarbonyl ($Fe(CO)_5$, > 99.99%), reference Fe_2O_3 (< 50 nm) and CuO (< 50 nm) were all obtained from Sigma-Aldrich. The aluminum nanopowder (~ 50 nm ALEX, 70 wt% active Al) used in the combustion test was purchased from the Argonide Corporation.

2.2. Aerosol Processing, Iron Oxide Coating and Materials Characterizations

The I_2O_5 nanoparticles were generated by the thermal decomposition of HIO_3 at ~ 290 °C [39] in the aerosol processing which was previously discussed in the introduction. The iron oxide coating was fulfilled by mixing $Fe(CO)_5$ vapor and the I_2O_5 aerosol stream in a furnace at 200 ºC. The carrier gas was air for the aerosol

processing while the iron pentacarbonyl vapor was carried by a controlled argon flow. The residence time of the whole process was ~ 8 seconds when the air flow rate is ~ 3.5 L/min. The final passivated I_2O_5 particles were collected on a HTTP membrane filter (0.4 μm pore, Millipore) and characterized by TEM (JEOL JEM 2100 FEG) coupled with EDS (Oxford INCA 250) line scan.

If iron pentacarbonyl completely turned into Fe_2O_3 and deposited on the I_2O_5 surface, the thickness of Fe_2O_3 layer is calculated to be 4.3 nm, 12 nm, 34 nm and 49 nm for the flow rates of argon at 26, 75, 210, and 300 sccm. The corresponding Fe/I molar ratios were determined to be 0.25, 1.8, 4.3 and 6.2 using a weight loss experiment which will be discussed in the following 2.3.1.

2.3. Combustion Performance Characterization

2.3.1. Thermite Sample Preparation

The reaction chemistry of the passivated I_2O_5 based thermite reaction can be written as follows:

$$(6a+10)Al+3[aFe_2O_3+I_2O_5]\rightarrow(3a+5)Al_2O_3+6aFe+3I_2\uparrow$$

$[aFe_2O_3+I_2O_5]$ is the formula of passivated I_2O_5 with the Fe/I molar ratio a. The "a" can be determined by the weight loss experiment where the I_2O_5 was fully decomposed at 600 ºC [39] with the help of a Sartorius SE2 Ultra Micro Balance (Sartorius AG). The appropriate amount of ALEX powder and the passivated I_2O_5 were weighed out and mixed in hexane, which were then sonicated for 20 min to ensure that the fuel and oxidizer powders were intimately mixed. The hexane was evaporated in the fume hood overnight. The dry powder was gently broken apart to obtain a loose powder before the combustion test.

2.3.2 Combustion Cell Test

A simultaneous pressure and optical measurements were conducted in a constant-volume combustion cell [38,40,41] to characterize the reactivity of the prepared thermite samples. Because the measurement is a relative experiment, both the pressurization rate and optical emission signals are usually reported along with reference oxidizers: Fe_2O_3 and CuO nanoparticles. In a typical combustion cell test, a ~25 mg thermite mixture with a correct stoichiometry, was placed in a combustion cell (constant-volume ~13 cm^3), and ignited by resistive heating with a loop shaped NiCr wire with a diameter of 0.010". The data collection was triggered by the rising optical signal after ignition. A fast time response piezoelectric pressure transducer attached to the cell was used to measure the transient pressure pulse. The optical emission was simultaneously collected by a lens tube containing a planoconvex lens (f = 50 mm). Both the pressure and optical signals were recorded by an oscilloscope. The pressurization rate is expressed as the peak pressure (KPa) divided by the pressure rise time (μs). The characteristic burn time of thermite in the combustion cell is arbitrarily represented by the full width at half-maximum (FWHM) of the recorded optical signal. The combustion cell is schematic depicted in Figure 6 and the details of the combustion cell test are given else in the previous publications of our lab [38,40,42].

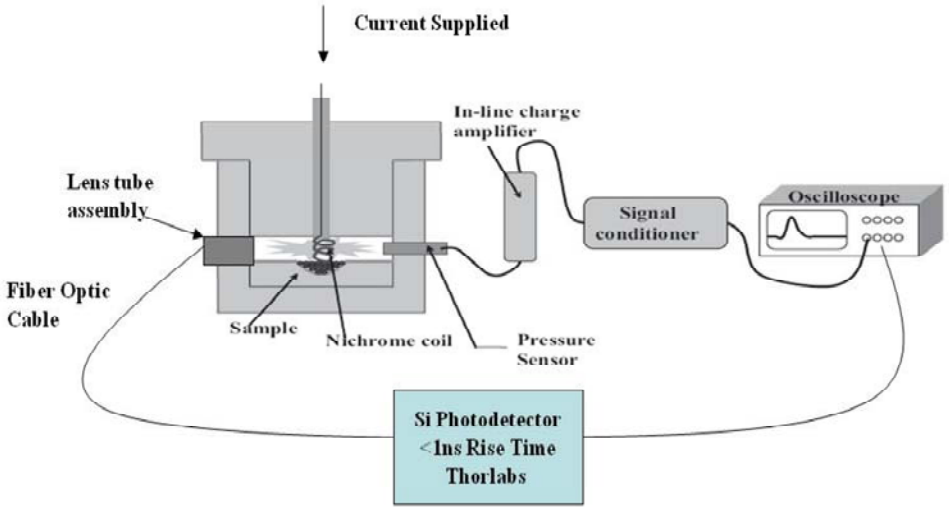

Figure 6. Schematic showing of combustion cell

2.3.3. Temperature-Jump/Time-Of-Flight Mass Spectrometry (T-Jump/TOFMS)

The condensed phase reaction kinetics measurements are usually performed using conventional thermal analysis techniques such as thermogravimetric analysis (TGA) and differential scanning calorimetry (DSC) [39]. However those measurements cannot provide critical information of fast reaction chemistry process like rapid heating. To evaluate the decomposition behavior of the passivated I_2O_5, a rapid heating experiment coupled to mass-spectrometry was employed. In these experiments a thin layer of passivated I_2O_5 sample is coated onto a 12 mm long, ~ 76 μm diameter platinum wire which could be rapidly resistively heated to 1800 K in 3 ms with a heating rate at ~ 5×10^5 K/s. The temporal measured wire resistances are used to determine the temporal filament temperature. The details of T-Jump/TOFMS experiment can be found in our previous papers [41,43].

2.3.4. High-Speed Imaging

High speed imaging of the wire tests were conducted under atmospheric conditions using a Vision Research Phantom® v12.0 high-speed digital camera at a resolution of 256×256 with a frame rate of 67065 fps (14.9 μs per frame).

3.Results and Discussions

3.1. The I_2O_5 Passivation

The I_2O_5 passivation was accomplished by using a controlled thermal decomposition of $Fe(CO)_5$ in air to in situ coat the I_2O_5 aerosol particles with a Fe_2O_3 layer. The basic concept is to do the chemical vapor deposition of Fe_2O_3 onto the surface of I_2O_5 nanoparticles, thus allowing for the core-shell passivated structure.

In the experimental setup shown in Figure 7, the precursor iodic acid was sprayed into the aerosol droplets which passed through the first silica-gel diffusion dryer and furnace. The first furnace was set to 290 °C to decompose HIO_3 aerosol stream to I_2O_5 nanoparticles [39]. The water produced in the decomposition was removed by silica-gel diffusion dryer to ensure no iodic acid but I_2O_5 to enter the second furnace.

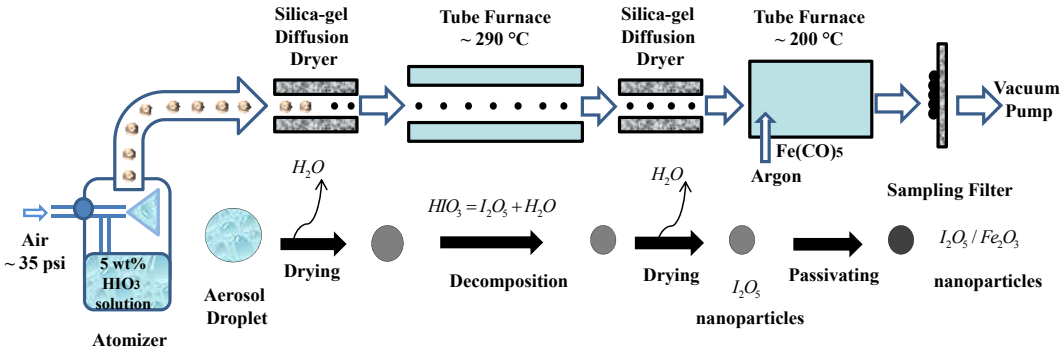

Figure 7. Experimental setup for I_2O_5 passivation

The $Fe(CO)_5$ vapor was carried by a controlled argon flow and decomposed to elemental iron and CO_2 [44] in the second furnace (~ 200 °C) where they were mixed with a constant flow of I_2O_5 nanoparticles.

3.2. The Passivated I_2O_5 Characterizations

The multiple techniques such as TEM, EDS line scan, and T-Jump MS, were utilized to characterize the size, structure, morphology and composition of the passivated I_2O_5 particles.

The iron pentacarbonyl was introduced into the second furnace with the argon flow rate at 26, 75 and 210 sccm. The related Fe/I molar ratios were determined using the weighing measurement to be 0.25, 1.8 and 4.3 respectively. The size, structure and morphology of particles were further examined by TEM with EDS line scans. Figure 8 (a) shows the representative TEM image of the final product with a Fe/I molar ratio of 0.25 obtained at the argon flow rate of 26 sccm. At these low concentrations we observed only the spherical smooth shell passivated particles with no evidence of homogeneous nucleated fine particles of iron oxide. The TEM images show the particles in some cases have a hollow like structure, resulting from heating by the electron beam of the microscope, which indicates an incomplete coating. In fact one can see in some cases iodine containing crystals in some hollow structured particles. Figure 8 (b) shows a TEM image of I_2O_5/Fe_2O_3 passivated oxidizer with a Fe/I molar ratio of 1.8. The particles have a mean diameter of ca. 200 nm. Closer scrutinization reveals a clear fractal structure that extends from the surface of particles, implying that some gas phase homogeneous nucleation of the iron oxide was taking place.

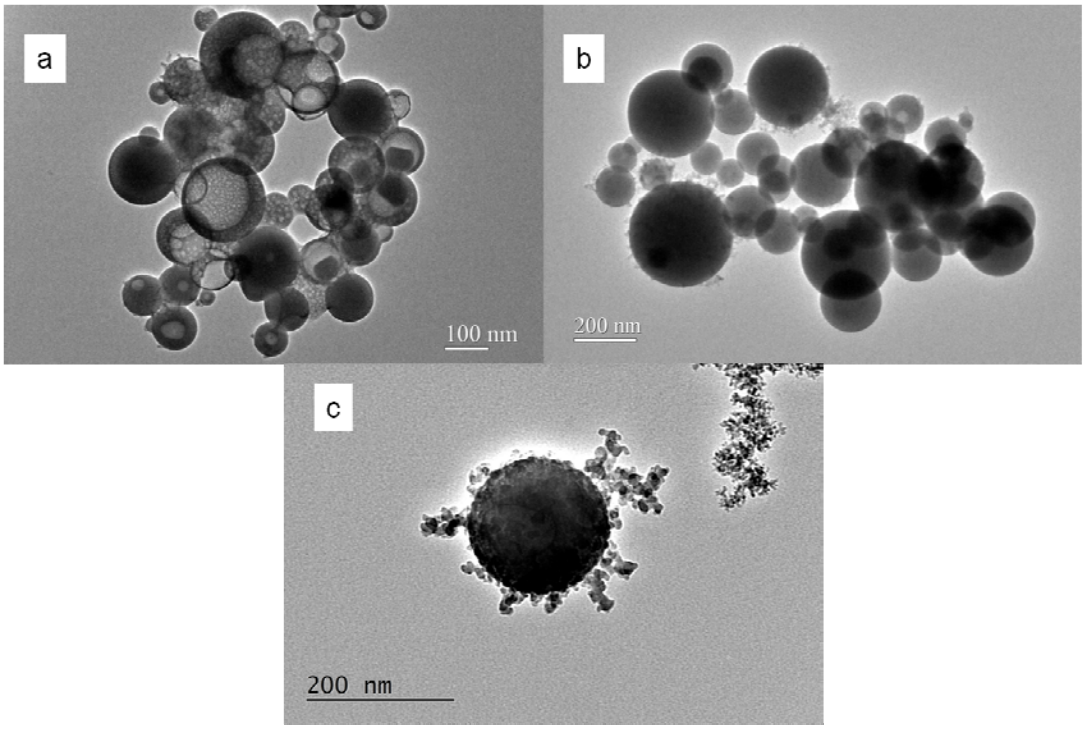

Figure 8. TEM images of passivated I_2O_5 particles with Fe/I molar ratio at: (a) 0.25; (b) 1.8; (c) 4.3

At a higher concentration of iron pentacarbonyl, corresponding to a Fe/I molar ratio of 4.3, the final product shows evidence of considerable homogeneous nucleation of the iron (which will subsequently be converted to iron oxide outside the reactor). Figure 8 (c) shows a passivated I_2O_5 particle, with a large fraction of fractal aggregates on the surface of the I_2O_5 particles. Figure 9 shows the TEM image of passivated oxidizer product (Fe/I molar ratio: 4.3) with an elemental line scan. As shown in Figure 9 (a), the obtained core/shell type particle has an iodine oxide core and an iron oxide shell. A cleared view of the core-shell material of the particle is seen in Figure 9 (b), whose image was taken after the elemental scan, which apparently caused sufficient heating to decompose the I_2O_5 and evaporate the I_2, revealing the remaining iron-oxide shell. The shell thickness appears close to the ~34

nm which was estimated assuming all the iron pentacarbonyl decomposed and ended up as iron oxide on the surface of I_2O_5 core particles.

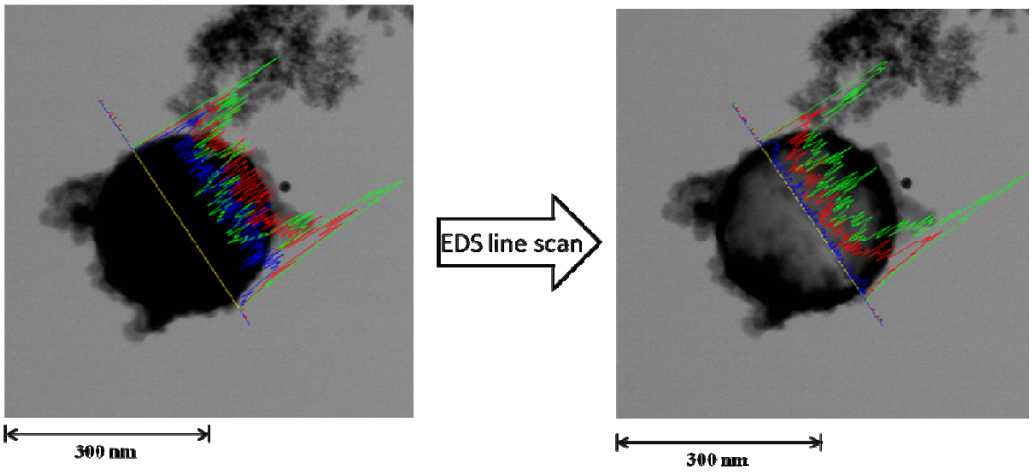

Figure 9. A TEM image of passivated I_2O_5 particle (Fe/I molar ratio: 4.3) with elemental profile (Green: Fe; red: O; blue: I)

(a) The elemental profile of a solid passivated I_2O_5 particle.

(b) The elemental profile of particle (a) after an EDS line scan.

The transient event of the passivated I_2O_5 decomposition was monitored by T-Jump/TOFMS when rapid heated. In a typical experiment, the materials were coated onto a platinum wire as a thin layer, which was rapidly heated up to ~1800 K at a rate of ~ 5×10^5 $K \cdot s^{-1}$. The species generated in the decomposition was monitored by a mass spectrometer. In the time resolved mass spectra of the passivated I_2O_5 shown in Figure 10, only O_2, I, I_2 and no IO_x species were observed. Note that in our previous work [45], we have found a significant amount of IO_x species in mass spectra of I_2O_5 sample exposed to the ambient air. The IO_x species are attributed to the decomposition of iodic acid, which is consistent with previous results of HIO_3 decomposition by using mass spectrometer [46]. In the mass spectra (Figure 10), we

didn't observe any IO_x species, indicating there is no iodic acid within the structure. Thus, pure I_2O_5 was passivated in the Fe_2O_3 shell.

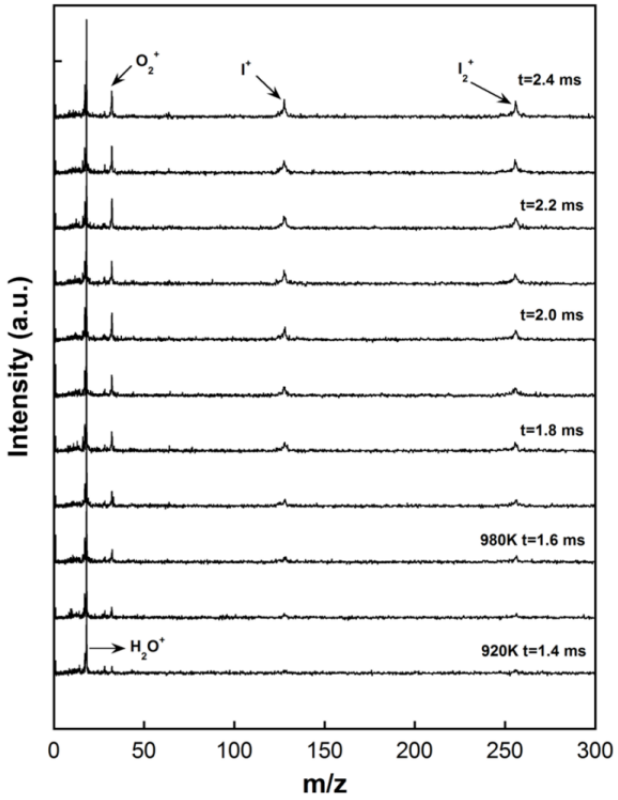

Figure 10. Time resolved mass spectra of the passivated I_2O_5 (Fe/I molar ratio: 4.3) under rapid heating. The heating pulse is ~ 3 ms and the heating rate is ~ 5×10^5 $K \cdot s^{-1}$.

3.3. Combustion Performance of "Al + (I_2O_5/Fe_2O_3)"

The reactive behavior of the prepared "Al + (I_2O_5/Fe_2O_3)" nanothermite was characterized by high-speed digital camera. The experiment was carried out at a high heating rate (~ 5×10^5 $K \cdot s^{-1}$) on a 76 μm diameter platinum wire, for which selected snapshots are shown in Figure 11. The iodine pentoxide-containing thermite system clearly shows a violent reaction over a period of ~ 2000 μs.

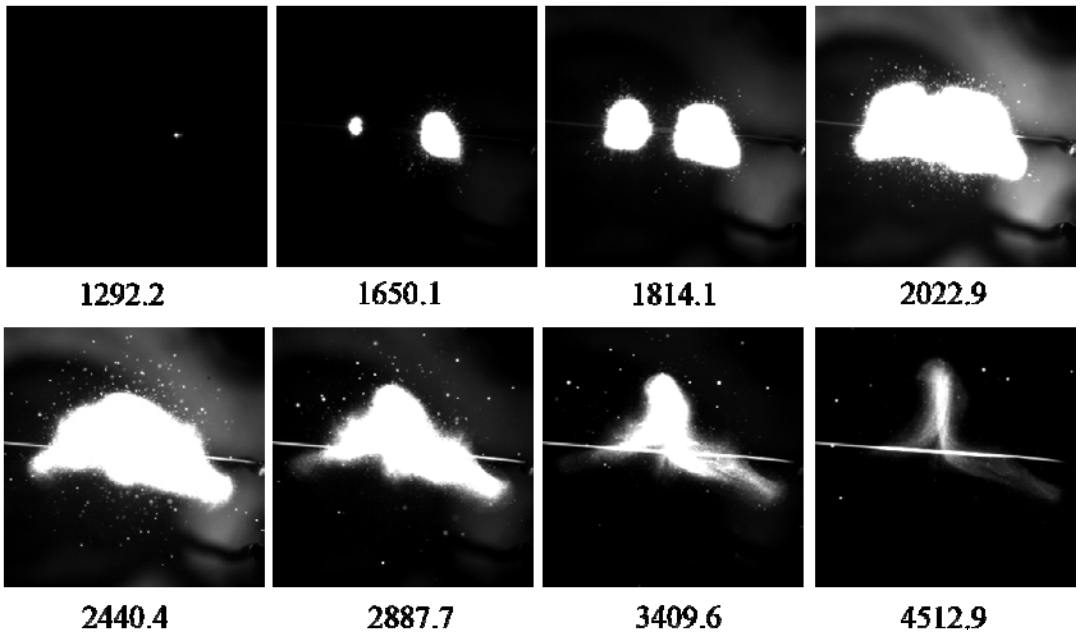

Figure 11. High speed images of "Al + (I_2O_5/Fe_2O_3)" (Fe/I molar ratio: 4.3) in the T-Jump/TOFMS. (Units: μs).

The relative combustion performance of "Al + (I_2O_5/Fe_2O_3)" thermite against the reference thermite "Al + nano-Fe_2O_3" and "Al + nano-CuO" was evaluated in a constant volume combustion cell. Table-1 summarizes the experimental results of pressure and optical emission for thermite samples prepared with different oxidizers. Clearly, the "Al + (I_2O_5/Fe_2O_3)" thermite with Fe/I molar ratio of 1.8 and 4.3 outperforms "Al + nano-Fe_2O_3" in both pressurization rate and transient peak pressure, and with shorter FHWM burning time. However, the formulated nanothermite does not exceed the performance of "Al + nano-CuO", when directed comparing their pressurization rates, as shown in Figure 12.

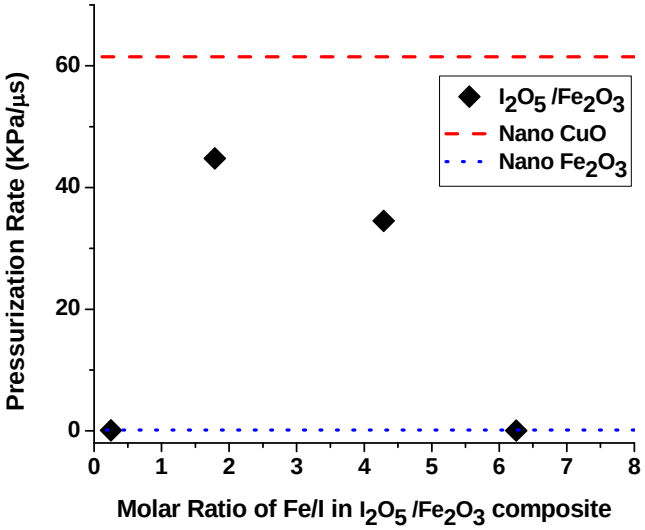

Figure 12. Pressurization rate for thermite samples prepared with I_2O_5/Fe_2O_3 with different Fe/I molar ratios in the composite particles. The nano-CuO and nano-Fe_2O_3 were used here as reference oxidizers.

In the previous publications in our lab, we have argued that the pressurization takes place as a result of releasing oxygen from oxidizer's decomposition, which occurs well before significant optical emission [38,42]. A nanothermite system like "Al + CuO" has a rapid pressure rise followed by an optical signal due to the rapid oxygen release of CuO [7,38]. This is consistent with Table 1, which illustrates that the time scale of optical emission of "Al + nano-CuO" is much longer than the pressure rise time. Unlike "Al + CuO", the pressure and optical signals of "Al + Fe_2O_3" occur almost concurrently in which the decomposition of Fe_2O_3 becomes the rate-limiting step [38,42].

Table 1. Combustion cell test data for thermite samples prepared with different oxidizers. All oxidizers were mixed with nano-Al powder (ALEX). Thermite sample was prepared with a specific stoichiometry assuming complete conversion of Al to Al_2O_3.

Oxidizers (w/nano-Al, φ=1)	Molar ratio of Fe/I	P_{rise} (KPa)	Pressure rise time (μs)	Pressurization Rate (KPa/μs)	FWHM burn time (μs)	Note
I_2O_5/Fe_2O_3	0.25	152	1530	0.0896	1910	Aerosol + iron pentacarbonyl
	1.8	1262	28	45.1	183	
	4.3	821	24	35.2	119	
	6.2	108	2970	0.0363	4280	
Nano-Fe_2O_3(ref.)	N/A	92.4	800	0.116	936	< 50 nm, Sigma-Aldrich
Nano-CuO(ref.)	N/A	800	13	61.5	192	

Note: The reported pressurization rate has an uncertainty of < 10% based on two runs.

In addition, we might moderate the thickness of the shell by varying the ratio of iron to iodine and evaluate the effect of shell thickness on combustion performance. The oxidizers with Fe/I molar ratio of 0.25 and 6.2 in Table-1 and Figure 13 show similar relative behavior as a poor "Al + Fe_2O_3" thermite; the pressure rise times are similar to the time scales of the optical emission, which indicates the pressure signal and the optical emission occurred almost concurrently. At low Fe/I molar ratios (0.25), the poor performance can be attributed to insufficient surface coverage to fully passivate I_2O_5. At the other extreme, a large excess of iron (Fe/I = 6.2) also serves to degrade performance, with reactive behavior even poorer than pure iron oxide.

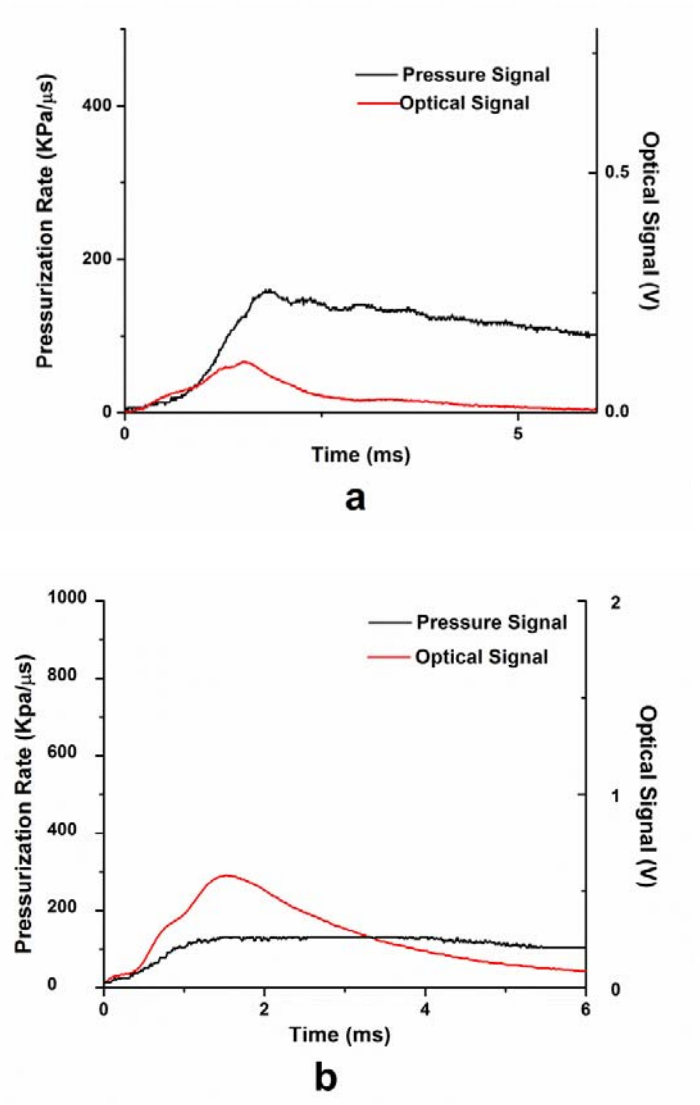

Figure 13. Pressure and optical signals for thermite samples prepared with I_2O_5/Fe_2O_3 with a Fe/I molar ratio of (a) 0.25 and (b) 6.2 in the combustion cell.

When the Fe/I molar ratio is 1.8 or 4.3, the thermites show a similar relative behavior as "Al + CuO", a rapid rising pressure signal followed by a prolonged optical signal (the pressure rise times are much shorter than FHWM burn times), as shown in Table-1 and Figure 14, indicating that the I_2O_5 nanoparticles are well passivated by Fe_2O_3 and have a similar burning mechanism as CuO. Thus the reactivity of Fe_2O_3/I_2O_5 passivated oxidizer can be tuned by varying the Fe/I ratio.

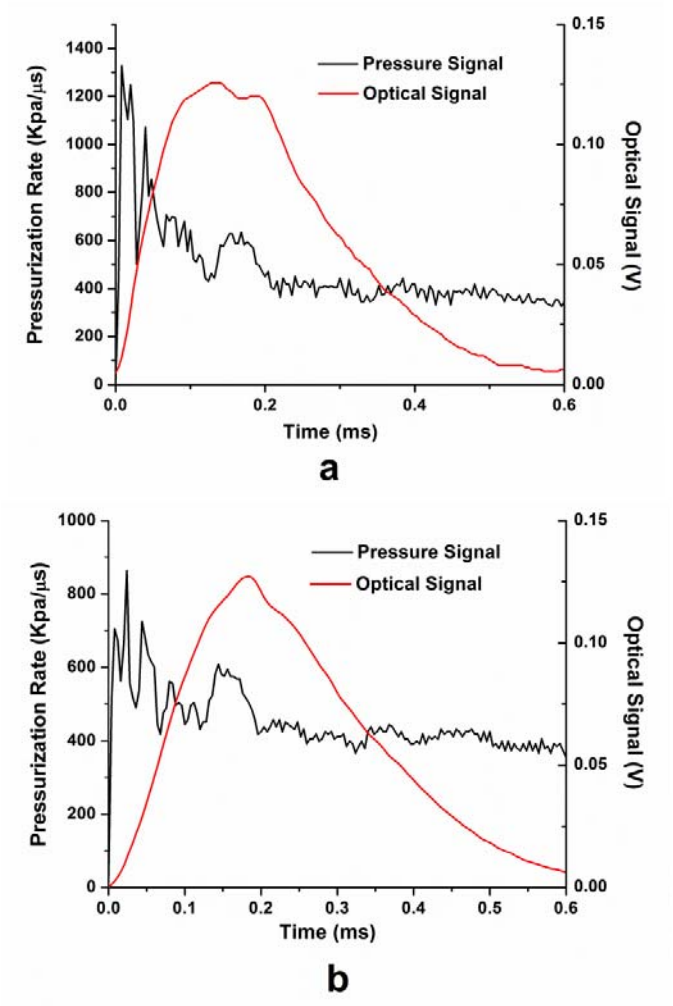

Figure 14. Pressure and optical signals for thermite samples prepared with I_2O_5/Fe_2O_3 with a Fe/I molar ratio of (a) 1.8, and (b) 4.3 in the combustion cell

3.4 The Long Term Stability Experiment

The long term stability experiment of the passivated I_2O_5 (Fe/I molar ratio: 4.3) was conducted by exposing the sample in the ambient air and measuring the weight change for ten days with a Sartorius SE2 Ultra microbalance. The results were listed in Table-2. RH (%), which means relative humidity, was monitored by an OMEGA HX15-W humidity indicator. The mass change percentage during ten days was obtained from the mass on Day-10 divided by that of Day-1. If I_2O_5 completely

hydrolyzes to HIO_3, the weight will be increased by around 5%. Our passivated I_2O_5 has a mass change of +1.6% indicating the product has very good stability during ten days' exposure to the ambient air.

Table-2. The long term stability experiment of passivated I_2O_5

Oxidizers	Molar ratio of Fe/I	The mass of the passivated I_2O_5/mg						The mass change percentage
		Day-1 RH=53.9	Day-2 RH=64.3	Day-3 RH=37.4	Day-4 RH=28.8	Day-5 RH=37.4	Day-10 RH=71.3	
I_2O_5/Fe_2O_3	4.3	31.750	32.311	32.311	32.313	32.300	32.270	+1.6%

4. Summary

In summary, we successfully passivated the highly hygroscopic I_2O_5 into iron oxide shell by an aerosol spray pyrolysis method coupled with chemical vapor deposition. The final material's core/shell structure was confirmed by TEM with EDS line scan. A significant oxygen and iodine release was observed in T-Jump MS, which further reveals its potential biocidal application. The reactivity of the passivated I_2O_5 based nanothermite can be tuned by varying the iron/iodine molar ratio using a controlled decomposition of iron pentacarbonyl. The coating thickness can be optimized for passivated I_2O_5 based nanothermite to perform similar to that of CuO in the combustion test.

Chapter 3: $Cu(IO_3)_2$ & $Fe(IO_3)_3$ for Potential Biocidal Nanoenergetic Applications

1. Introduction

As discussed in the introduction, Iodine-producing reactive materials have potential application in the destruction of biological warfare agents like spores [31].

The copper iodate, $Cu(IO_3)_2$, when heated up to a temperature of 450 ºC, produces copper oxide with oxygen and iodine release [35].

$$2Cu(IO_3)_2 \rightarrow 2CuO + 2I_2 \uparrow + 5O_2 \uparrow$$

Iodine works as biocide for biological agent defeat [39] while CuO is a strong oxidizer commonly used in aluminum-based nanothermite formulations [38], which makes $Cu(IO_3)_2$ an ideal candidate for potential biocidal energetic applications. Similarly, $Fe(IO_3)_3$ may decompose to release iodine and oxygen gas [36]:

$$4Fe(IO_3)_3 \rightarrow 2Fe_2O_3 + 6I_2 \uparrow + 15O_2 \uparrow$$

In this chapter, the anhydrous copper iodate microparticles, $Cu(IO_3)_2$, and iron iodate nanorod, $Fe(IO_3)_3$, were successfully synthesized by a simple co-precipitation method and they were confirmed by XRD. The significant amount of oxygen and iodine release was observed in T-Jump mass spectra when copper iodate was decomposed. The obtained copper iodate particles, even though in micron size, exhibited a violent reaction when formulated as an oxidizer with nano-aluminum fuel in the high speed imaging. The next step will be focused on how to obtain $Cu(IO_3)_2$ nanoparticles which embrace the promise of better combustion performance.

2. Experimental Details

2.1. Materials

Iodic acid (HIO_3, 99.5%), Iron(III) nitrate nonahydrate ($Fe(NO_3)_3 \cdot 9H_2O$, ACS reagent, ≥98%), copper (II) nitrate trihydrate ($Cu(NO_3)_2 \cdot 3H_2O$, puriss. p.a., 99-104%), reference Fe_2O_3 nanopowder (< 50 nm) and CuO nanopowder (< 50 nm) were all purchased from Sigma-Aldrich. The 50 nm ALEX nano-aluminum powder (70 wt% active) in combustion test was obtained from the Argonide Corporation.

2.2. Iodate Synthesis

The iron iodate and copper iodate powders were prepared by co-precipitation of metal nitrate and iodic acid in the aqueous solution. Firstly, the precursors were separately dissolved in DI water, which was followed by stirring for 2 h at room temperature. The metal nitrate solution was then slowly added into the iodic acid solution with vigorous stirring. The precipitation occurred immediately and the color of the precipitate is pale green for iron iodate and light blue for copper iodate. The reaction chemistry is shown below:

$$Fe(NO)_3 + 3HIO_3 \rightarrow Fe(IO_3)_3 \downarrow + 3HNO_3$$

$$Cu(NO)_2 \cdot 3H_2O + 2HIO_3 \rightarrow Cu(IO_3)_2 \cdot H_2O \downarrow + 2HNO_3 + 2H_2O$$

After that the whole batch was heated up and kept at 80 °C for 4 hours with vigorous stirring. Finally the suspensions were filtered (30μm) and washed with DI water and acetone. The obtained powders, iron iodate (yellow-green) and copper iodate (light blue), were dried in the fume hood overnight at room temperature.

2.3. XRD Characterization

The metal iodate powders were characterized by a Bruker C2 Discover Diffractometer which uses a CuKa source with a HiStarr (GADDS) detector. All samples detected were loose powders. The obtained XRD spectra were compared with the standard spectra in the XRD spectra database to make sure the right materials were obtained.

2.4. Combustion Performance Evaluation

2.4.1. Thermite Sample Preparation

The reaction chemistry of the thermite reaction for iron iodate and copper iodate is as follows:

$$4Al + Cu(IO_3)_2 \rightarrow 2Al_2O_3 + Cu + I_2$$
$$12Al + 2Fe(IO_3)_3 \rightarrow 6Al_2O_3 + 2Fe + 3I_2$$

As described in previous chapters, the appropriate amount of nano-aluminum fuel and the iodate salts was weighed out, mixed in hexane and then sonicated for 20 min to ensure an intimate mixing. The hexane was evaporated in the fume hood overnight. The dry powder was gently broken apart to obtain a loose powder before the combustion test.

2.4.2. Combustion Cell Evaluation

The combustion cell evaluation was conducted in a constant-volume combustion cell and the pressurization rate was employed to characterize the reactivity of the prepared thermite samples. In a typical experiment, a thermite sample powder (~25 mg) with the correct stoichiometry, was placed in a constant-volume (~13 cm^3) combustion cell, and ignited by resistive heating with a NiCr wire. Both the pressure

and optical signals were recorded. The details of the combustion cell test can be found in our prior publications [38,40,42].

2.4.3. Temperature-Jump/Time-Of-Flight Mass Spectrometry (T-Jump/TOFMS)

To evaluate the decomposition behavior of the iodates, a rapid heating experiment coupled to mass-spectrometry was employed. In this experiment a thin layer of sample is coated onto a platinum wire which could be rapidly resistively heated to ca. 1800 K in 3 ms when the heating rate is ~ 5×10^5 K/s. The decomposition event can be monitored in the mass spectrometer to probe transient species evolution. The details of T-Jump/TOFMS experiment can be found in our previous papers [41,43].

2.4.4. High-speed imaging

High speed imaging of the wire tests were conducted under atmospheric conditions using a Vision Research Phantom® v12.0 high-speed digital camera at a resolution of 256×256 with a frame rate of 67065 fps (14.9 μs per frame).

3. Results and Discussions

3.1 Copper Iodate Particles

The anhydrate copper iodate particles were obtained by a calcination of copper iodate hydrate for 10 min at a temperature of 240ºC. The final compound was confirmed to be copper iodate by XRD (Ref#: PDF 70-1844) as shown in Figure 15: the black plot is the synthesized copper iodate while the red plot is the standard copper iodate. The particle size is around 20 μm as shown in SEM (Figure 16).

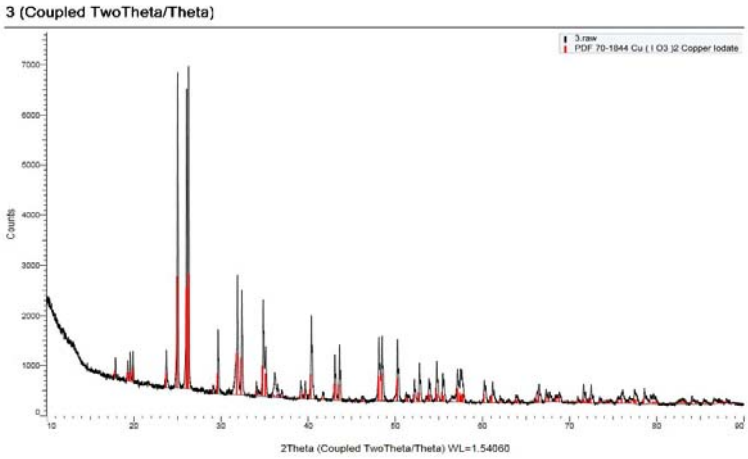

Figure 15. XRD of anhydrous $Cu(IO_3)_2$ (Ref#: PDF 70-1844)

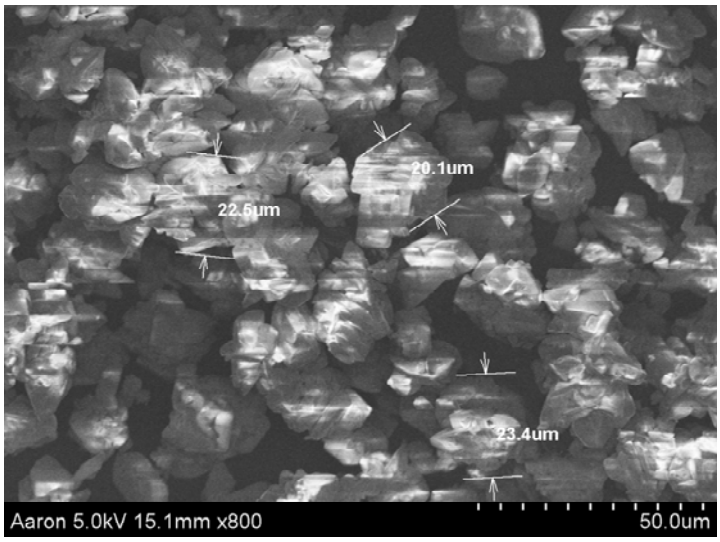

Figure 16. SEM image of anhydrous $Cu(IO_3)_2$ particles

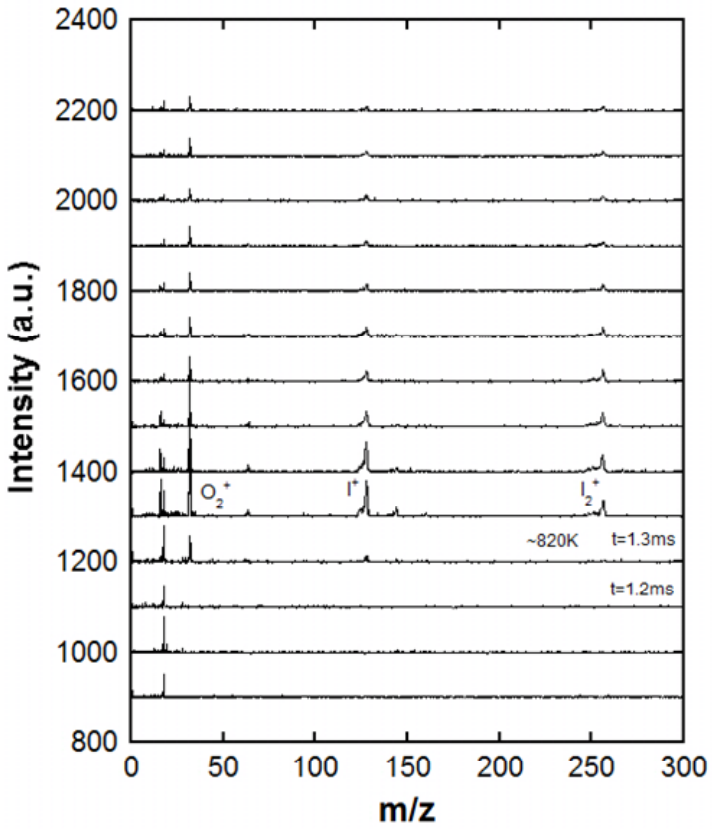

Figure 17. T-Jump mass spectra of anhydrous $Cu(IO_3)_2$ decomposition

The T-Jump mass spectra in Figure 17 shows that the $Cu(IO_3)_2$ started to decompose when heated up to the temperature of ~820 K. As shown in the spectra, a significant amount of oxygen and iodine species were released after the decomposition.

The $Cu(IO_3)_2$ is expected to have two stages of oxygen release when it is decomposed [35].

$$2Cu(IO_3)_2 \rightarrow 2CuO + 2I_2 \uparrow + 5O_2 \uparrow \cdots\cdots \text{(d)}$$

$$4CuO \rightarrow 2Cu_2O + O_2 \uparrow \cdots\cdots \text{(e)}$$

Only the products from the reaction (d) were observed in T-Jump mass spectra in Figure 17. The possible reason is that the gas released in the first oxygen release stage

blows off the solid CuO particles so that the second decomposition stage (e) cannot happen.

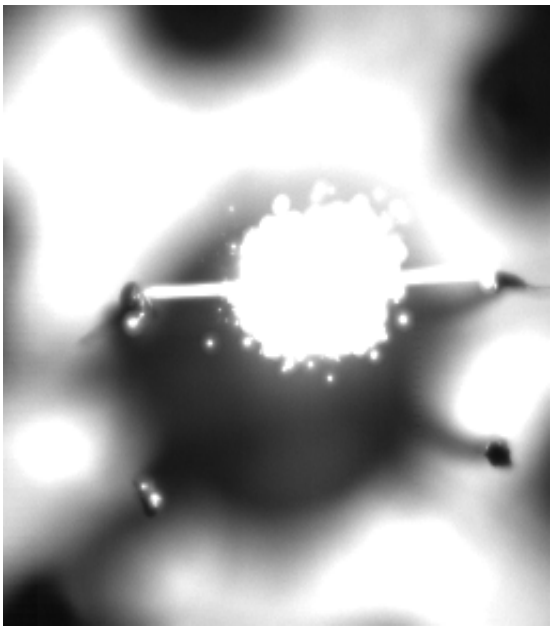

Figure 18. Hi-speed imaging of the burning behavior of Al/$Cu(IO_3)_2$ on platinum wire

High-speed imaging of the reactive behavior was carried out at on a platinum wire (76 μm diameter) at a high heating rate of ~ 5×10^5 $K \cdot s^{-1}$, which is shown in Figure 18. The copper iodate-based thermite system "$4Al + Cu(IO_3)_2 \rightarrow 2Al_2O_3 + Cu + I_2$" clearly shows a violent reaction although the particle size is around micron.

3.2 Iron Iodate Nano-rods

The final $Fe(IO_3)_3$ powders were shown to be nanosized rods in TEM (Figure 19) and it was confirmed to be iron iodate by XRD (Ref#: PDF 70-0146) as shown in Figure 20.

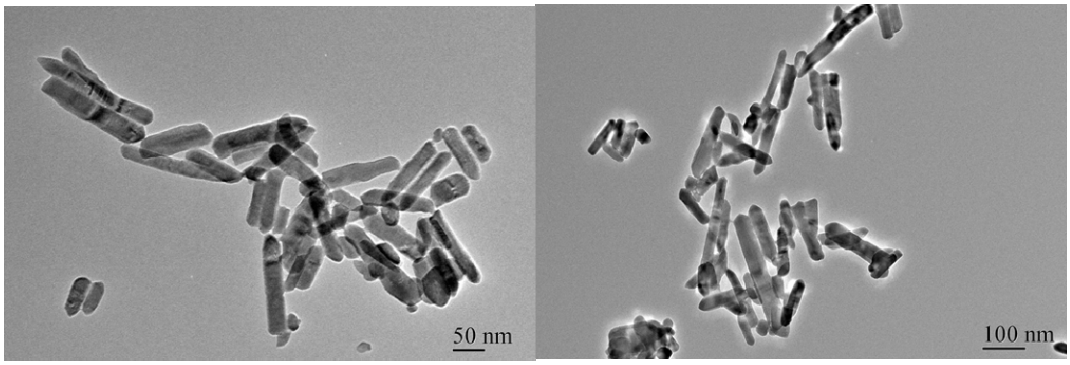

Figure 19. TEM images of iron iodate nano-rods

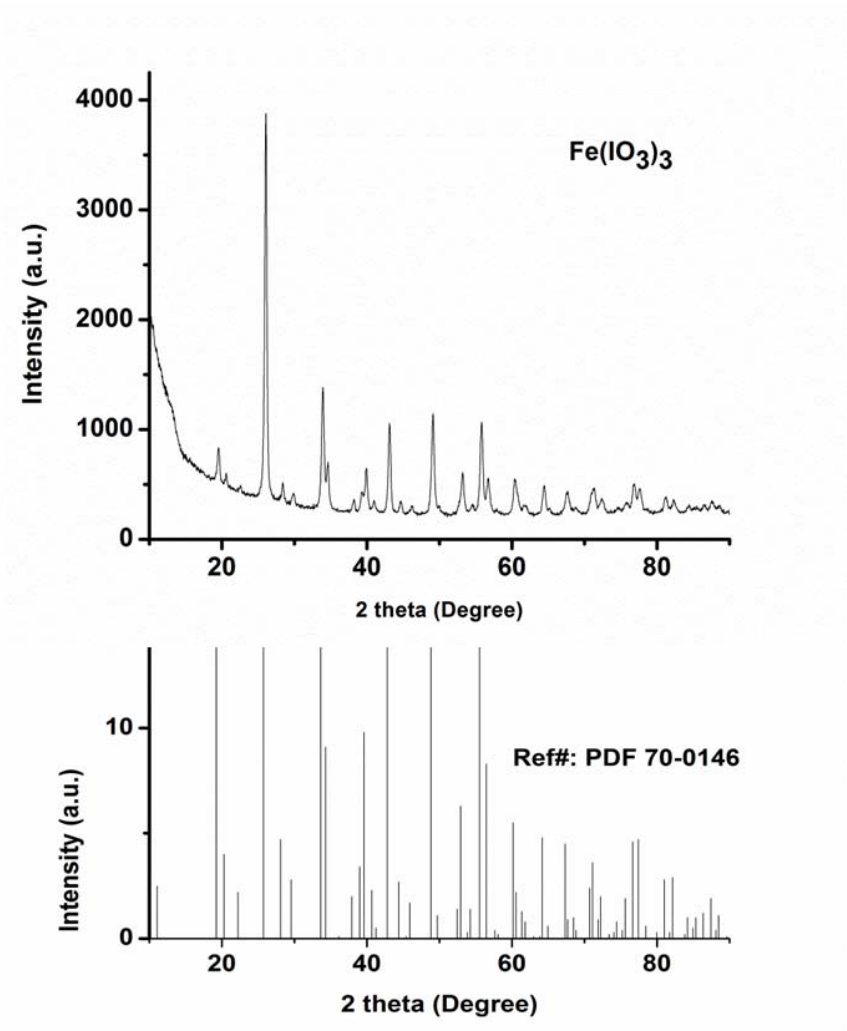

Figure 20. XRD of $Fe(IO_3)_3$ (Ref#: PDF 70-0146)

However, the decomposition mechanism of $Fe(IO_3)_3$ is not fully understood yet. Galez *et.al* noticed that in the TGA test, the weight loss of $Fe(IO_3)_3$ is expected to be 86% if its decomposition follows the reaction chemistry below [36]:

$$4Fe(IO_3)_3 \rightarrow 2Fe_2O_3 + 6I_2 \uparrow + 15O_2 \uparrow$$

But the experimental value they obtained was around 70%, which is lower than the theoretical value, indicating the decomposition mechanism of iron iodate needs further studies.

3.3 Combustion Cell Test Results

Table-3. Combustion cell test data for thermite samples prepared with different oxidizers[a]

Oxidizers (w/Al, φ=1)	**P_{rise} (KPa)**	**Pressure rise time (μs)**	**Pressurization Rate (KPa/μs)**	**FWHM burn time (μs)**	**Note**
Nano-$Fe(IO_3)_3$	167	1007	0.157	691	nanorod, co-precipitation
Micro-$Cu(IO_3)_2$	111	3240	0.0326	3660	~20 μm, co-precipitation
Micro-CuO	152	732	0.208	514	<5 μm, 98% , Sigma-Aldrich
Micro-Fe_2O_3	51.7	8350	0.00619	4394	<5 μm, ≥99%, Sigma-Aldrich
Nano-CuO	800	13	61.5	192	<50 nm, Sigma-Aldrich
Nano-Fe_2O_3	92.4	800	0.116	936	<50 nm, Sigma-Aldrich

[a] All six oxidizers were physically mixed with ALEX nano-aluminum powder. Thermite sample was prepared with a specific stoichiometry assuming complete conversion of Al to Al_2O_3. Note: The reported pressurization rate has an uncertainty of <10% based on two runs.

The Table-3 listed the combustion cell test data for thermite samples prepared with different oxidizers. Compared to nano-Fe_2O_3, the nano-$Fe(IO_3)_3$ performed slightly better in the pressure rise, pressurization rate and burn rate because $Fe(IO_3)_3$ has additional oxygen and iodine release when decomposed. Although the micro-$Cu(IO_3)_2$ exhibited a violent reaction when formulated into the nanothermite reaction in high speed imaging, it has lower pressure rise and smaller pressurization rate than micro-CuO, probably due to the fact that micro-$Cu(IO_3)_2$ (~ 20 μm) is larger than micro-CuO (< 5 μm).

4. Summary

The synthesis of iron iodate and copper iodate particles was attempted by the simple co-precipitation method. The final materials were confirmed by XRD compared with the standard XRD database. The significant amount of oxygen and iodine release was observed in T-Jump mass spectra when copper iodate was decomposed. The obtained copper iodate microparticles showed a violent reaction when employed as an oxidizer with nano-aluminum fuel in the high speed imaging and combustion cell.

Chapter 4: Conclusion and Future Work

1.Conclusion

The conventional energetic materials have relatively lower energetic density and slower burn rate. The nanothermite, highly exothermic, greatly decreases both mass and heat diffusion limits by reducing the reactants to the nanoscale dimensions, showing superior reactive properties to conventional energetic materials in the combustion. Iodine-containing oxidizers, releasing elemental iodine when reacting with aluminum fuel in the thermite reaction, embrace the promise of the ideal candidate for biocidal agent defeat.

The objective of this thesis is to prepare iodine-containing oxidizers for nanothermite reaction, which has potential applications to neutralize biological weapons. Chapter 2 describes a novel gas phase-assisted aerosol processing to coat the highly hygroscopic I_2O_5 with an outer layer of iron oxide. The Fe_2O_3 shell not only protects I_2O_5 from the moisture in the ambient air but also actively participates in the thermite reaction. The synthesized passivated I_2O_5, with an optimal coating thickness, exhibited excellent combustion performance. With the help of T-Jump mass spectrometer the significant release of iodine species was observed in the decomposition event of passivated I_2O_5 when rapidly heated. Chapter 3 demonstrates two promising metal iodates particles prepared by a simple co-precipitation method. The copper iodate microparticles and iron iodate nano-rods were obtained and characterized by multiple techniques. The copper iodate particles, even though in

micron size, exhibited a violent reaction when formulated in the aluminum based nanothermite reaction. Because the copper iodate has additional oxygen and iodine release compared to its metal oxide counterparts when decomposed, it embraces a promise of better combustion performance with biocidal capabilities.

2. Future Work

2.1 Improved I_2O_5/Fe_2O_3 Nanocomposite Synthesis

In Chapter 2, the synthesized I_2O_5/Fe_2O_3 nanocomposite oxidizer demonstrated an excellent combustion performance and a significant amount of elemental iodine release when formulated into the nano-aluminum based thermite; however, this was only observed when Fe/I molar ratio was tuned to 1.8 or 4.3, indicating that the particles have much more iron than iodine. By increasing the size of core I_2O_5 nanoparticle, the iodine content in each final particle could be increased, which could further improve the combustion and biocidal performance of the nanocomposite material. In the introduction and background part, we mentioned that the obtained particle size depends on the atomized droplet size and starting solution concentration. By either lowering the precursor concentration or increasing the droplet size, the larger particle size could be obtained. And switching to other types of atomizers which generate bigger droplets could be also utilized to achieve this goal.

2.2 Extension of the Passivation Strategy to other Hygroscopic Materials

Besides I_2O_5, the similar passivation strategy in Chapter 2 can be extended to passivate other sensitive, hygroscopic materials. For example, AN (Ammonium Nitrate) is a promising rocket propellant oxidizer because AN, unlike the widely used AP (Ammonium Perchlorate), is one of the cheapest compounds but also it produces

completely environmental friendly products that are smokeless and chlorine free [47]. However, its hygroscopic property restricted its application in rocket propellants. Our passivating method can be utilized to coat AN with an iron oxide layer to protect it from eroding by humidity.

2.3 Copper Iodate Nanoparticle Synthesis

In Chapter 3, the anhydrous copper iodate microparticles, $Cu(IO_3)_2$, were successfully synthesized by co-precipitation method with a further calcination and the final microparticles showed excellent combustion performance in high speed imaging and significant amount of iodine and oxygen release in mass spectra when decomposed, which indicates that copper iodate is a promising candidate for biocidal energetic applications. The future research will be focused on how to decrease the particle size to nanoscale.

One way could be to add stabilizing agent, usually surfactant, at the point of, or after, precipitation to control the final particle size. The common stabilizing agents are polyvinyl alcohol (PVA), polyvinylpyrrolidone (PVP), dextran, albumin, and oleic acid. The organic protecting shell can be removed by washing in an appropriate solvent or by decomposition at elevated temperature [48].

Another way may be to control the reaction rate of the co-precipitation. We could use syringe to add copper nitrate solution into iodic acid solution in co-precipitation. The addition rate might be tuned by a syringe pump and several experiments could be done to check the correlation of addition rates with the final particle sizes. After that, an optimal addition rate may be obtained to prepare the copper iodate nanoparticles.

The ultrasonic reactor probe might be able to help the co-precipitation batch to generate smaller sized particles [49]. The ultrasonic bath assisted co-precipitation was prelimilarily employed to synthesize copper iodate particles which turned out to be composed of particle with multiple sizes (Figure 21). The possbile reason is because the frequency of the ultrasonic bath is low and unstable. The ultrasonic reactor probe with stable and higher frequency might be able to produce well-dispersed copper nanoparticles.

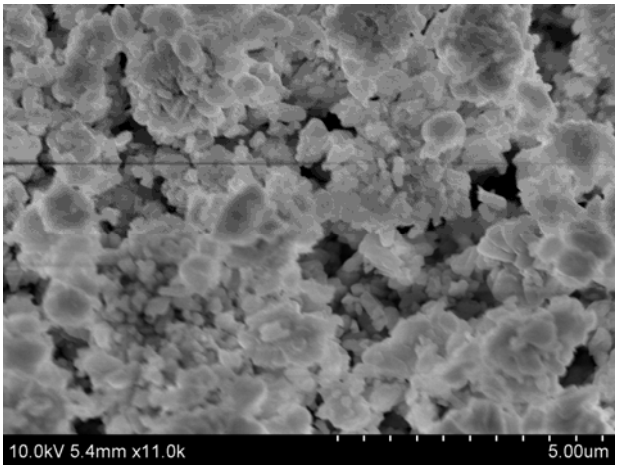

Figure 21. The SEM of copper iodate particles synthesized by ultrasonic bath assisted co-precipitation

References

[1] Rossi, C.; Zhang, K.; Estève, D.; Alphonse, P.; Thailhades, P.; Vahlas, C. *J. Microelectromech. Syst.* **2007**, *16*, 919-931.

[2] ICT Database of thermochemical va*lues. 2001, Pfinztal, Germany:* Fraunhofer Inst*itut für Chemische Technologie.*

[3] CRC Handbook of Chemistry and Physics. 2002: Hampden Data Services Ltd.

[4] Fischer and Grubelich in: 32nd AIAA/ASME/SAE/ASEE Joint Propulsion Conference Lake Buena Vista, FL, 1996; Lake Buena Vista, FL, 1996.

[5] Rossi, C.; Estève, A.; Vashishta, P. *J. Phys. Chem. Solids* **2010**, *71*, 57-58.

[6] Kim, S.H.; Zachariah, M. R. *Adv. Mater.* **2004**, *16*, 1821-1825.

[7] Jian, G.; Liu L.; Zachariah, M. R. *Adv. Funct. Mater.* **2013**, 23, 1341-1346.

[8] Malchi, J. Y.; Foley, T. J.; Yetter, R. A. *ACS Appl. Mater. Interfaces* **2009**, *1*, 2420-2423.

[9] Yan, S.; Jian, G.; Zachariah, M. R. *ACS Appl. Mater. Interfaces* **2012**, *4*, 6432-6435.

[10] Séverac, F.; Alphonse, P.; Estève, A.; Bancaud, A.; Rossi, C. *Adv. Funct. Mater.* **2012**, *22*, 323-329.

[11]http://www.nationaldefensemagazine.org/archive/2012/November/Pages/TopFive-ThreatstoNationalSecurityintheComingDecade.aspx (accessed in Nov. 2013)

[12] Inglesby, T.; Henderson, D. A.; Bartlett, J. G.; Ascher, M. S.; Eitzen, E.; Friedlander, A. M.; Hauer, J.; McDade, J.; Osterholm, M. T.; O'Toole, T.; Parker, G.; Perl, T. M.; Russell, P. K.; Tonat, K. *J. Am. Med. Assoc* **1999**, *281*, 1735-1745.

[13] http://news.nationalpost.com/2011/12/07/biological-weapons-threat-growing-clinton-says/ (accessed in Nov. 2013)

[14] Zhang, S.; Badiola, C.; Schoenitz, M.; Dreizin, E. L. *Combust. Flame* **2012**, *159*, 1980−1986.

[15] Zhang, S.; Schoenitz, M.; Dreizin, E. L. *J. Phys. Chem. C* **2010**, *114*, 19653−19659.

[16] Grinshpun, S.A.; Adhikari, A.; Yermakov, M.; Reponen, T.; Dreizin, E.; Schoenitz, M.; Hoffmann, V.; Zhang, S. *Environ. Sci. Technol.* **2012**, *46*, 7334−7341.

[17] Fischer, D.; Klapötke, T.; Stierstorfer, J. *Z. Anorg. Allg. Chem.* **2011**, *637*, 660−665.

[18] Clark, B. R.; Pantoya, M. L. *Phys. Chem. Chem. Phys.* **2010**, *12*, 12653−12657.

[19] Sullivan, K.; Piekiel, N.; Chowdhury, S.; Wu, C.; Johnson, C.; Zachariah, M. R. *Combust. Sci. Technol.* **2011**, *183*, 285−302.

[20] Sullivan, K.; Wu, C.; Piekiel, N.; Gaskell, K.; Zachariah, M. R. *Combust. Flame* **2013**, *160*, 438−446.

[21] Grinshpun1, S.A.; Li, C.; Adhikari, A.; Yermakov, M.; Reponen, T.; Schoenitz, M.; Dreizin, E.L.; Hoffmann, V.; Trunov, M. *Aerosol Air Qual. Res.* **2010**, *10*, 414-424.

[22] Setlow, P. *J. Appl. Micorbiol* **2006**, *101*, 514-525.

[23] Boissiere, C.; Grosso, D.; Chaumonnot, A.; Nicole, L.; Sanchez, C. *Adv. Mater.* **2011**, *23*, 599-623.

[24] Okuyama, K.; Abdullah, M.; Lenggoro, I. W.; Iskandar, F. *Adv. Powder Technol.* **2006**, *17*, 587-611.

[25] Bayvel, L.; Orzechowski, Z. *Liquid Atomization*, Taylor & Francis US, **1993**.

[26] Pang, J. B.; Stuecker, J. N.; Jiang, Y. B.; Bhakta, A. J.; Branson, E. D.; Li, P.; Cesarano, J.; Sutton, D.; Calvert, P.; Brinker, C. J. *Small*, **2008**, *4*, 982-989.

[27] Okuyama, K.; Lenggoro, I. W.; Tagami, N.; Tamaki, S.; Tohge, N. *J. Mater. Sci.*, **1997**, *32*, 1229-1237.

[28] Kim, S. H.; Liu, B. Y. H.; Zachariah, M. R. *Chem. Mater.*, **2002**, *14*, 2889-2899.

[29] Kodas, T. T.; Hampden-Smith, M. J. *Aerosol Processing of Materials*, Wiley-VCH, New York, **1999**.

[30] Okuyama, K.; Lenggoro, I. W. *Chem. Eng. Sci.*, **2003**, *58*, 537-547.

[31] Johnson, C. E.; Higa, K. T. *MRS Proc.* 2013, 1521.

[32] Wiberg, E.; Wiberg, N.; Holleman, A. F. *Inorganic Chemistry*, 1st ed.; Academic Press: New York, **2001**; p 465.

[33] Earnshaw, A.; Greenwood, N. *Chemistry of Elements*, 2nd ed.; Butterworth-Heinemann: Oxford, **1997**; p 852.

[34] Feng, J.; Jian, G.; Liu, Q.; Zachariah, M. R. *ACS Appl. Mater. Interfaces* **2013**, *5*, 8875-8880.

[35] Stern, K.H. *High Temperature Properties and Thermal Decomposition of Inorganic Salts with Oxyanions*, **2001**, CRC Press, 1 edition.

[36] Galez, C; Mugnier,Y; Bouillot, J; Lambert, Y; Le Dantec, R. *J. Alloy. Compd.* **2006**, *416,* 261–264.

[37] Prakash, A.; McCormick, A. V.; Zachariah, M. R. *Nano Lett.,* **2005**, *5*, 1357-1360.

[38] Wu, C.; Sullivan, K.; Chowdhury, S.; Jian, G.; Zhou, L.; Zachariah, M. R. *Adv. Funct. Mater.,* **2012**, *22*, 78-85.

[39] Farley, C.; Panoya, M. J. *Therm. Anal. Calorim.* **2010**, *102*, 609-613.

[40] Prakash, A.; McCormick, A.; Zachariah, M. R. *Adv. Mater.* **2005**, *17*, 900-903.

[41] Zhou, L.; Piekiel, N.; Chowdhury, S.; Zachariah, M. R. *Rapid Commun. Mass Spectrom.* **2009**, *23*, 194-202.

[42] Sullivan, K.; Zachariah, M. R. *J. Propul. Power* **2010**, *26*, 467-472.

[43] Jian, G.; Piekiel, N.W.; Zachariah, M. R. *J. Phys. Chem. C* **2012**, *116*, 26881-26887.

[44] Giesen, A.; Herzler, J.; Roth, P. *J. Phys. Chem. A* **2003**, *107*, 5202-5207.

[45] Jian, G.; Chowdhury, S.; Feng, J.; Zachariah, M. R. In *8th U. S. National Combustion Meeting*, Park City, Utah, United States, May 19-22, 2013.

[46] Studier, M.H.; Huston, J. L. *J. Phys. Chem.*, **1967**, *71(2)*, 457-459.

[47] Oommen, C.; Jain, S. R. *J. Hazard. Mater.* **1999**, *67*, 253-281.

[48] Chan, K-Y; Ding, J; Ren, J; Cheng, S; and Tsang, K-Y. *J. Mater. Chem.* **2004**, *14*, 505-516.

[49] Wu, S.; Sun, A.; Zhai, F.; Wang, J.; Xu, W.; Zhang, Q.; Volinsky, A. A. *Mater. Lett.* **2011**, *65*, 1882-1884.